International Journal of Heat and Mass Transfer 51 (2008) 5642–5649

Contents lists available at ScienceDirect

International Journal of Heat and Mass Transfer

journal homepage: www.elsevier.com/locate/ijhmt

Three-dimensional microscopic freezing and thawing behavior of biological tissues revealed by real-time imaging using confocal laser scanning microscopy

Hiroshi Ishiguro [a,*], Takashi Horimizu [b]

[a] Graduate School of Life Science and Systems Engineering, Kyushu Institute of Technology, 2-4 Hibikino, Wakamatsu-ku, Kitakyushu, Fukuoka 808-0196, Japan
[b] Graduate School of Engineering Mechanics, University of Tsukuba, 1-1-1 Tennoudai, Tsukuba, Ibaraki 305-8573, Japan

ARTICLE INFO

Article history:
Received 30 October 2007
Received in revised form 4 April 2008
Available online 12 June 2008

Keywords:
Biological tissues
Ice crystals
Freezing
Thawing
Confocal laser scanning microscope
Real-time 3D imaging

ABSTRACT

Three-dimensional behavior of ice crystals and cells during freezing and thawing of biological tissues was investigated microscopically in real time by using a confocal laser scanning microscope (CLSM) and a fluorescent dye. Fresh white meat of chicken was stained in physiological saline, and then frozen and thawed under two different thermal protocols. The CLSM noninvasively produced tomograms of the tissues to clarify the pattern of freezing, the morphology of ice crystals in the tissues, and the interaction between ice crystals and cells. The results were compared and correlated with observed histological changes in the post-thaw tissues.

1. Introduction

Freezing and thawing of biological tissues are fundamental phenomena in cryopreservation and cryosurgery. Cryopreservation is the preservation of biological tissues *in vitro* by freezing, and cryosurgery is the destruction of biological malignant tissues *in vivo* by freezing [1,2]. Cryopreservation is commonly utilized in the medical field, agriculture, fishery, stock raising, and food engineering, and is useful in preserving tissue-engineered equivalents. These applications will benefit from fundamental research of bioheat transfer.

Survival of biological tissue after freezing and thawing depends on the type of tissue, the thermal history during cooling and warming, and the type and concentration of cryoprotectant used in the cryopreservation. Criteria that consumers use to determine the quality of food include texture, taste, smell, and nutritional value. However, detailed phenomena during freezing and thawing and the mechanisms responsible for injuries incurred during freezing and for the protection by cryoprotectants are not well understood [3–5]. The thermal history and chemical additives of biological tissue are macroscopic handling conditions that control the viability and quality of the tissue. These conditions directly determine the microscopic mechanical and chemical conditions surrounding the cells in the tissues. They also affect the biologically large molecules (e.g., proteins and lipids), water, and ice at the molecular level. Investigation of the microstructure of biological tissue during freezing and thawing under these various macroscopic handling conditions will help clarify the mechanisms responsible for the freezing injuries and for the protection by cryoprotectants.

The freezing and thawing of tissue generally proceed transiently and spatially in three-dimensions (3D). Therefore, 3D observation in real time is required to understand the details of the microstructure of tissues during freezing and thawing. For such observation, commonly used optical and electron microscopy have limitations. One limitation is that these techniques require fixation of the sample; consequently, the same sample cannot be monitored during freezing and thawing [6–8]. Another limitation is that they produce only 2D images. For example, real-time observation of a single layer of cells (e.g., epidermis of an onion) by using optical microscopy yields only a 2D image averaged in the direction of thickness of the sample [9].

By contrast, confocal laser scanning microscopy (CLSM) with a fluorescent dye is a noninvasive method that produces 3D optical tomograms of biological materials for high spatial-resolution without fixation or slicing of a sample. This method was applied by Ishiguro and Koike to visualize the 3D behavior of ice crystals and cells during the directional solidification of red blood cell suspensions [10,11] and to clarify the effect of a cryoprotectant and cooling rate on the microstructure.

In this study, this CLSM/dye method for real-time 3D observation was applied to clarify the 3D behavior of ice crystals and cells during the freezing and thawing of biological tissues. Fresh white meat (muscle tissue) of chicken was used as the material and

* Corresponding author. Tel.: +81 93 695 6026; fax: +81 93 695 6005.
E-mail address: ishiguro@life.kyutech.ac.jp (H. Ishiguro).

0017-9310/$ - see front matter © 2008 Elsevier Ltd. All rights reserved.
doi:10.1016/j.ijheatmasstransfer.2008.04.019

Nomenclature

AO	acridine orange
CLSM	confocal laser scanning microscope
CT	connective tissues
H	cooling rate (°C/min)
IC(ex)	extracellular ice crystals
IC(in)	intracellular ice crystals
MF	muscle fibers (muscle cells)
T	temperature (°C)
t	time from start of cooling (min)
W	warming rate (°C/min)
x	distance in horizontal direction perpendicular to muscle fibers (μm)
y	distance in parallel direction to muscle fibers (μm)
z	distance upward in vertical direction from sample upper surface (μm)

acridine orange as the dye. The pattern of freezing, the morphology of the ice crystals in the tissue, and the interaction between ice crystals and cells were investigated for two different thermal protocols. The results were compared and correlated with observed histological changes in tissues due to freezing and thawing.

2. Experimental materials

Fresh white meat (second pectoral muscle) of chicken was selected as the experimental material due to its transparency for fluorescence visualization and to its common use as food. Two pieces of white meat (each about 35 g in weight) was removed from a 40- to 45-day-old broiler (from Arbor Acres, Japan; about 2.0 kg after blood was removed by draining) immediately after slaughter. The meat was muscle tissue with homogeneous structure consisting of a bundle of muscle fibers (muscle cells) connected by connective tissues (Fig. 1), and each muscle fiber consisted of a bundle of myofibrils. The meat was stored at 4 °C for about 1 h, and then a sample (about $10 \times 10 \times 3$ mm) with original smooth surface (needed for visualization by CLSM) was removed carefully by using a microtome blade. The sample was then placed in physiological saline (0.154 M NaCl) containing acridine orange (AO) (0.4 mg/ml) at 4 °C and then left undisturbed for between 90 and 120 min to stain the sample.

3. Experimental apparatus and methods

Microscopic behavior of the ice crystals and cells in the tissues during the freezing and thawing was imaged in 3D in real time by using the CLSM/dye method and the temperature of the sample was controlled by using a cryostage.

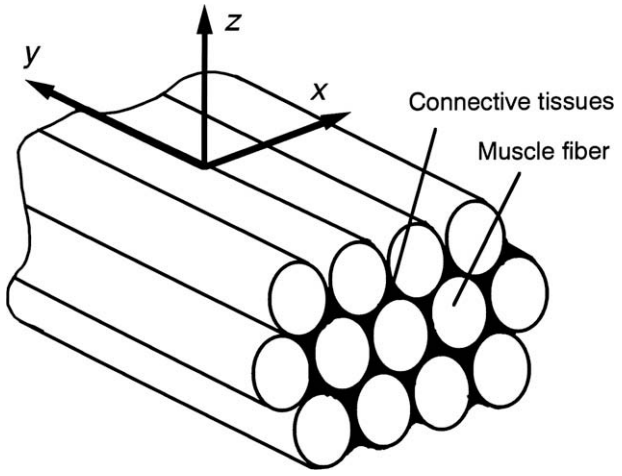

Fig. 1. Structure of tissues and coordinate system.

3.1. Cryostage

Fig. 2 shows a schematic of the cryostage attached to the CLSM and shows the coordinate system. The tissues were frozen and thawed on the cryostage at a uniform temperature according to the thermal protocol (see Section 3.2). The cryostage consisted of an aluminum (Al) block and a copper (Cu) plate (1.5 mm thick) that was lightweight (about 100 g in weight) for rapid vertical movement. The temperature at the cryostage surface was controlled by cooling with liquid nitrogen and by heating with a micro heating element. The sample was placed between a glass microslide (0.8–1.0 mm thick) and a glass coverslip (0.12–0.17 mm thick) so that the direction of muscle fibers was parallel to the x–y section and vertical to the x–z section with the original smooth surface of the sample upward. Good thermal contact between the microslide and the surface of the Cu plate was achieved by ethanol injected into a very thin gap between them.

3.2. Thermal protocols during freezing and thawing

The Cu-plate temperature was controlled between room temperature and a minimum temperature of −50 °C at a predetermined thermal protocol, which is defined as cooling-rate and warming-rate at the cryostage surface. The microstructure of the tissues during the freezing and thawing was imaged for two thermal protocols: (a) slow cooling (1 °C/min) and rapid warming (∼100 °C/min) and (b) rapid cooling (∼100 °C/min) and rapid warming (∼100 °C/min). The sample was maintained at the minimum temperature for 15 min. The rapid cooling rate and rapid warming rate are the attainable maximum rates for the cryostage used in this study and are defined as the time-averaged values between 10 °C and −50 °C. A new sample was prepared in every experiment and the experiments were repeated four or five times for each protocol.

3.3. Confocal laser scanning microscopy (CLSM)

A CLSM has two confocal pinholes and consequently has higher spatial-resolution, particularly a smaller depth of focus, compared with a typical optical microscope. The CLSM (Leica erect-type,

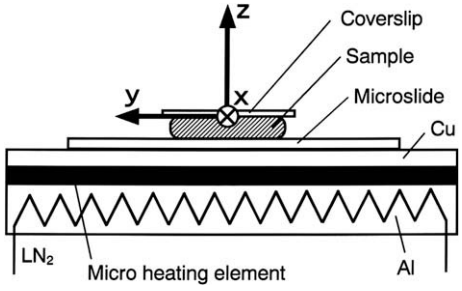

Fig. 2. Schematic of cryostage and coordinate system.

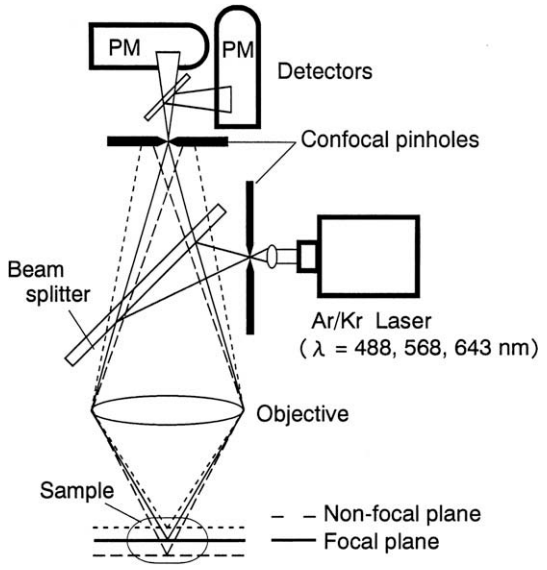

Fig. 3. Schematic of confocal laser scanning microscope (CLSM).

TCS4D) used in this study (Fig. 3) had an argon–krypton laser (488 nm, 568 nm, and 643 nm wavelengths; 25 mW maximum power output at each wavelength) and two photomultipliers for simultaneous detection of fluorescence at two different wavelengths. The CLSM was connected to a workstation for image acquisition, storage, and processing. Scanning by the laser beam across a horizontal (x–y) section of the sample combined with the vertical movement (z-direction) of the cryostage produced continuous, noninvasive, 3D optical tomograms. For good-quality images, the scanning time was set at 4.0 s per 512×512 pixel frame on either a horizontal or a vertical section.

3.4. Visualization using fluorescent dye

For fluorescence imaging, the tissues were stained with AO ($C_{17}H_{20}N_3Cl$, 301.8 in molecular weight). In previous studies, AO was used to stain red blood cell suspensions [10,11]. AO has the following characteristics:

(a) Maximum-excitation wavelength of 492 nm (blue) and two maximum-emission wavelengths of 530 nm (green) for monomers and 640 nm (red) for dimers.
(b) Monomer in solution and dimer when absorbed into a cell membrane.

When stained with AO, unfrozen solution generates green fluorescence, and cells generate red or yellow fluorescence. Ice does not generate fluorescence because during freezing of tissue, AO is not trapped in the ice, and thus ice crystals appear black. Therefore, ice crystals, cells, and unfrozen solution can be distinguished by their different colors. In the visualization images of the tissues, green areas corresponding to the unfrozen solution were not distinct because the tissues contained much smaller amounts of solution in the extracellular region than did the cell suspensions.

The moving distance of the focus of laser in the z-direction in the sample during the vertical movement of the cryostage is different from the moving distance of the focus in air due to the difference in refractive index between these optical mediums (sample and air). Furthermore, this difference in distance depends on the numerical aperture of the objective. Therefore, the former moving distance was obtained by correcting the latter moving distance equivalent to a moving distance of the sample in the z-direction, based on the refractive index of the sample solution (physiological saline) and the numerical aperture of the objective.

3.5. Evaluation of histological changes

After the tissues without fluorescence staining were frozen and thawed, they were fixed with formalin, treated with paraffin, and finally stained with masson-trichrome or hematoxylin-eosin. In general, with this staining method, the morphological structure of cells and tissues can be identified and discriminated based on their color. With hematoxylin-eosin, cell nuclei are stained shades of blue or indigo, and cytoplasm and connective tissues are stained shades of red or pink, whereas with masson-trichrome, connective tissues and mucus are stained blue, and cytoplasm and nucleus are stained red.

4. Results and discussion

4.1. Temperature change in tissues during freezing and thawing

The region observed by CLSM is limited to a depth of 100 μm from the top of the sample. Because the sample was warmed or cooled by controlling the temperature at the cryostage surface, temperature variation at the top of the sample with time differed from that at the cryostage surface due to the heat capacity, latent heat, and heat conduction in the sample. Therefore, the temperature of the sample during cooling and warming was measured using small-diameter (50 μm) thermocouples. Fig. 4 shows the changes in temperature as a function of time at the start of cooling at $t = 0$ min.

4.1.1. Temperature change during rapid cooling and rapid warming

Fig. 4a shows the temperature variation with time at the cryostage surface and at the upper and lower surfaces of the sample.

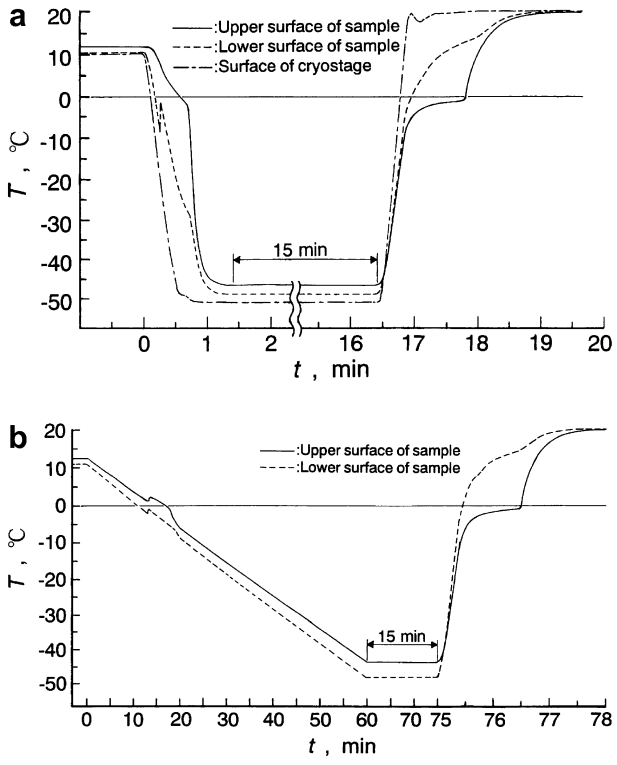

Fig. 4. Changes in temperatures during cooling and warming (a) rapid cooling and rapid warming ($H = 100$ °C/min, $W = 140$ °C/min) (b) slow cooling and rapid warming ($H = 1.0$ °C/min, $W = 140$ °C/min).

After a rapid decrease in temperature at the cryostage surface from 10 °C to −50 °C, the temperatures at both surfaces of the sample decreased with each characteristic delay. At the same moment, the upper surface of the sample, which was farthest from the cryostage surface, had the higher temperature. The temperature at the lower surface of the sample showed a spiked temperature-rise near t = 15 sec due to supercooling and the subsequent release of latent heat, and then until about t = 40 s, the temperature showed a delayed decrease due to the release of latent heat in the freezing process. The temperature at the upper surface of the sample showed a longer delay in temperature drop. Following this delay, the temperature of both surfaces of the sample decreased rapidly due to near completion of the freezing.

After the sample was maintained at the minimum temperature for 15 min, its temperature recovered finally to about 20 °C with a rapid increase at the cryostage. The temperature of the both surfaces of the sample showed a delay in temperature-rise near 0 °C, where a large amount of ice had thawed. The delay tendency at the upper surface of the sample was more pronounced (i.e., longer delay). For both surfaces, after the delay, the temperature increased rapidly due to near completion of the thawing.

Thus, the temperature in the sample underwent a complicated change as a function of time, depending on the location in the sample. The region observed by the CLSM was limited to near the top of the sample, whereas the region used to evaluate the histological changes was deeper within the sample, near the center. However, the microstructure observed in this limited region during the freezing and thawing should be representative of the sample because the structure of the tissues within the section was homogeneous and the tissues had roughly the same thermal history (particularly, the cooling rate). The results of histological change in the tissues due to freezing and thawing support this assertion (see Section 4.2.3). Here, the cooling/warming rate of the sample could only be roughly represented by that at the cryostage surface.

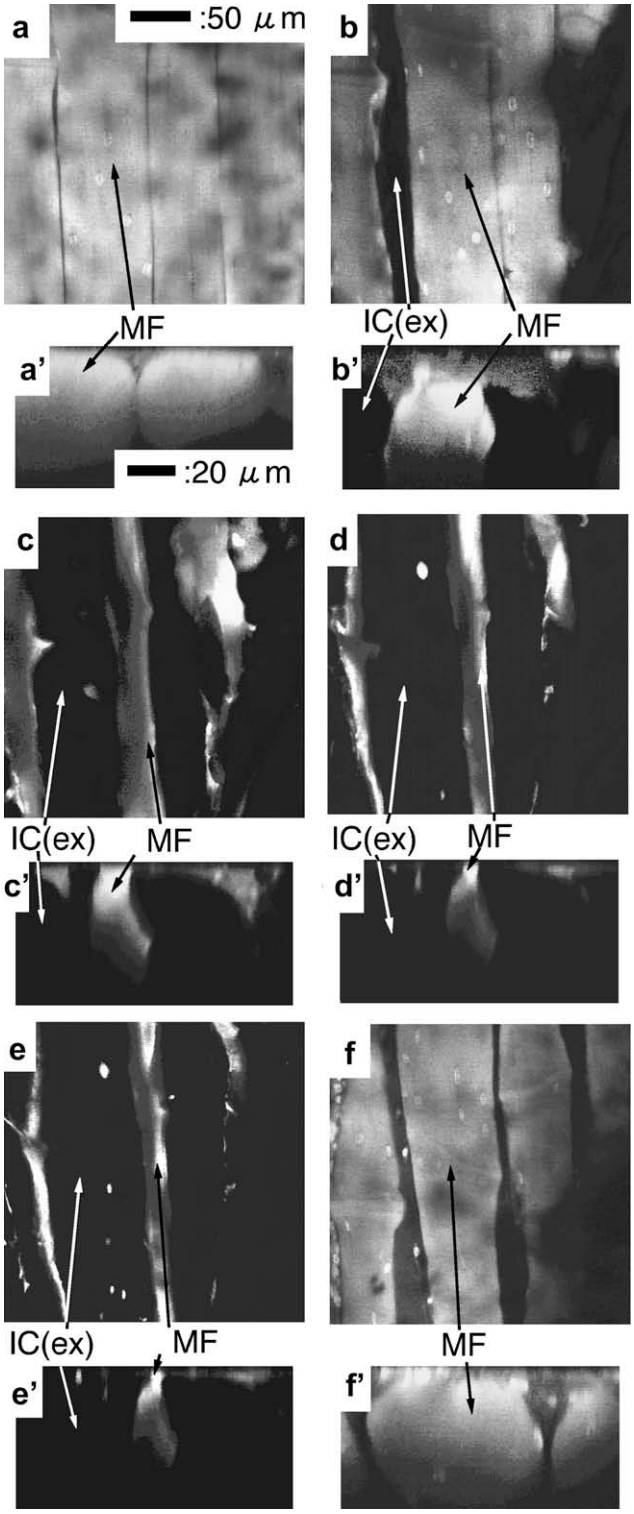

Fig. 5. Ice crystals and tissues during slow cooling and rapid warming (H = 1.0 °C/min, W = 130 °C/min) (a) 10 °C (14.0 °C) (before freezing), (b) −10 °C (−1.2 °C), (c) −11 °C (−5.0 °C), (d) −22 °C (−16.5 °C), (e) −50 °C (−42.4 °C), (f) 10 °C (12.9 °C) (after thawing).

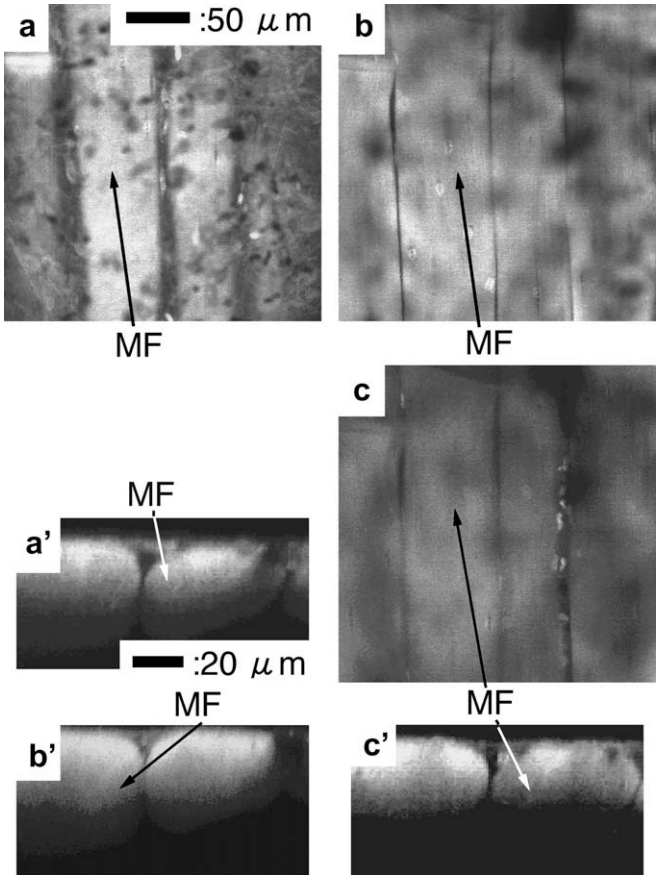

Fig. 6. Tissues before freezing for thermal protocol in Fig. 5 (a) z = −11.5 μm, (b) z = −28.7 μm, (c) z = −43.1 μm, (a′) y = 79.1 μm, (b′) y = 2.6 μm, (c′) y = −125.0 μm.

4.1.2. Temperature change during slow cooling and rapid warming

Fig. 4b shows the temperature variation with time at the upper and lower surfaces of the sample. (Note the scale change of the time axis before and after $t = 75$ min.) After a slow decrease in temperature at 1.0 °C/min at the cryostage surface, the temperatures at both the upper and lower surfaces of the sample showed a temperature rise caused by the release of latent heat due to the growth of ice crystals near 0 °C. Except for this temperature rise, the decrease in the temperature of the sample coincided with the decrease in temperature at the cryostage. Therefore, the cooling rate of the sample could be represented by that at the cryostage surface.

The change in temperature of the sample during the rapid warming after the slow cooling was similar to that after the rapid cooling (Section 4.1.1).

4.2. Microstructure of tissues during freezing and thawing

For each thermal protocol, a series of x–y (horizontal) and x–z (vertical) tomograms were continuously taken (using CSLM) before the freezing, at the minimum temperature, and after the thawing. A total of 50 x–y tomograms (512 × 512 pixels) with an area of 250 μm × 250 μm were taken at equally spaced intervals of 2.0 or 3.0 μm in the z-direction, and 50 x–z tomograms (512 × 512 pixels) with an area of 125 μm × 125 μm at equally spaced intervals of 5.1 μm in the y-direction. In addition, one set of x–y and x–z tomograms were taken every minute during the slow cooling.

Representative results from the imaging of the 3D microstructure are shown here as images of the x–y and x–z sections. Although the original images showed different colors for the ice crystals, for cells in the tissues, and for unfrozen solution, the images shown here are black-and-white photographs, where ice crystals appear black and muscle fibers appear gray. The tomograms designated by letters (a, b, c, etc.) are the x–y section images, and the tomograms designated by letters with apostrophes (a′, b′, etc.) are the x–z section images. In the x–y section images, the longitudinal and lateral directions correspond to the y- and x-directions (upward direction corresponds to $y > 0$), respectively, with the origin ($x = y = 0$ μm) located in the center of the image. The x–z section images show the central part (-62.5 μm $< x <$ 62.5 μm) of the x–y section image, and represent a depth of 100 μm at the most from the top of the sample.

In the figures, the temperature of the cryostage surface is shown, and that of the upper surface of the sample is shown as reference (in parentheses).

4.2.1. Behavior of ice crystals and tissues during slow cooling and rapid warming

The typical pattern of freezing during slow cooling was extracellular freezing. Fig. 5 shows representative time-series images of a sample during slow cooling and rapid warming (x–y section image at about $z = -30$ μm, and x–z section image at $y = 0$ μm), and Figs. 6–8 show detailed tomograms before the freezing, at the minimum temperature, and after the thawing, respectively.

Before freezing (Figs. 5a and 6), the muscle fibers about 60 or 70 μm in width (one muscle fiber is one cell) were adhered lengthwise to each other. In the images, cell nuclei (small spots) and strips of striated muscles can also be identified.

During the cooling, first the tissues went through supercooling to some degree, for lack of ice nuclei in the tissues, and then ice

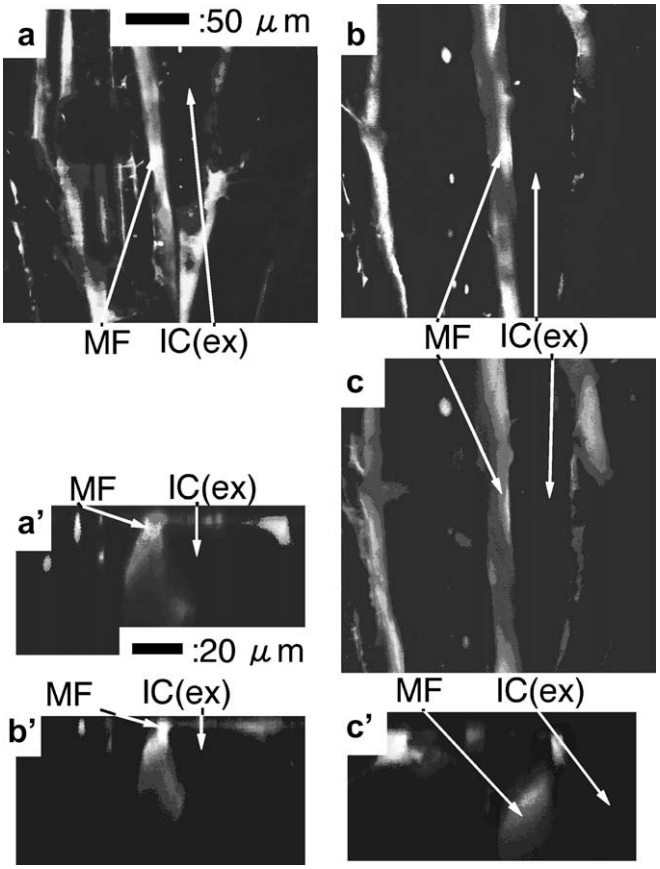

Fig. 7. Ice crystals and tissues at minimum temperature for thermal protocol in Fig. 5 (a) $z = -17.4$ μm, (b) $z = -34.8$ μm, (c) $z = -41.8$ μm, (a′) $y = 63.8$ μm, (b′) $y = 2.6$ μm, (c′) $y = -125.0$ μm.

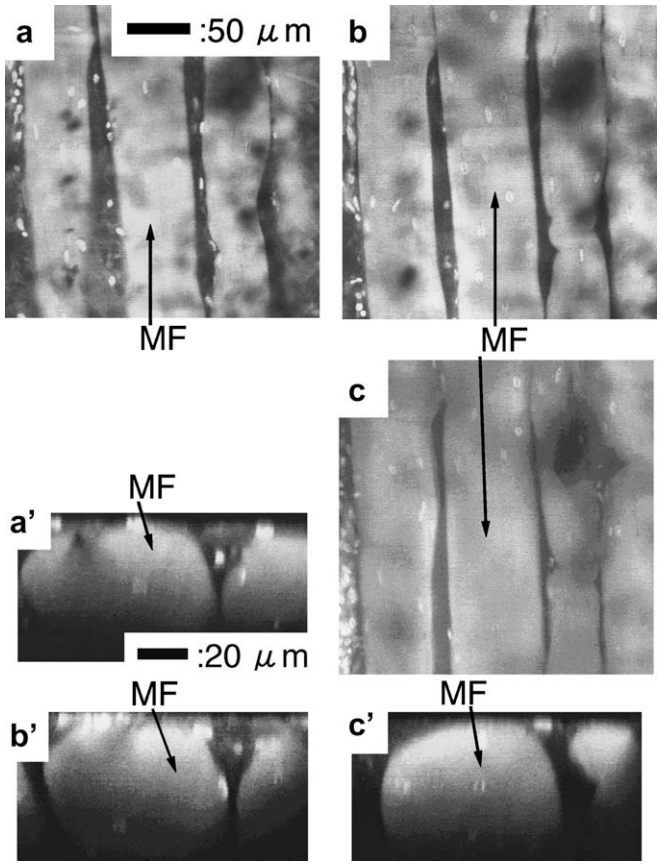

Fig. 8. Ice crystals and tissues after thawing for thermal protocol in Fig. 5 (a) $z = -19.1$ μm, (b) $z = -26.7$ μm, (c) $z = -45.8$ μm, (a′) $y = 109.7$ μm, (b′) $y = 2.6$ μm, (c′) $y = -53.6$ μm.

crystals appeared. Ice crystals first formed in the lower part of the sample where the temperature was lower due to the temperature difference across the sample. When the temperature decreased further, ice crystals appeared near the upper part of the sample where the temperature was higher. In Fig. 5b, ice crystals appeared between the muscle fibers and then grew, eventually tearing the fiber apart (connective tissue between the muscle fibers). The growth of these extracellular ice crystals (ice crystals between the muscle fibers) caused the muscle fibers to become dehydrated and to shrink, and thus the muscle fibers between the ice crystals decreased in diameter and became deformed. As the ice crystals grew with further decrease in temperature, the muscle fibers continued to shrink (Fig. 5c and d). However, the changing rates in the volumes of ice crystals and muscle fibers slowed due to the concentration of unfrozen solution in the tissues. The volumes of ice crystals and muscle fibers remained relatively unchanged, in the temperature range from −22 °C (Fig. 5d), which is near the eutectic point of physiological saline, to −50 °C (Fig. 5e). The ice crystals were similar in width to that of the muscle fibers in the *x*-direction, and had solid–liquid interfaces of relatively smooth shape. The decrease in the width of the muscle fibers by about 70 to 80% (compare Fig. 5a and e) indicates the degree of shrinkage of these fibers.

At the minimum temperature, extracellular ice crystals were observed similarly at different depths (Fig. 7a–c). The shrinkage and deformation of the muscle fibers along with the growth and morphology of ice crystals were quite pronounced and occurred in 3D.

During the warming, the ice crystals thawed and finally disappeared (Figs. 5f and 8). Simultaneously, the muscle fibers recovered in volume to some degree due to the inflow of water, into which ice dissolved, into the fibers. However, fibers did not recover to their original volume. After the thawing, adjoining muscle fibers remained torn due to extracellular ice crystals, irreversible cracks remained, and fibers remained deformed. The morphology of cracks and muscle fibers during warming occurred in 3D.

4.2.2. Behavior of ice crystals and tissues during rapid cooling and rapid warming

Fig. 9a–c shows detailed tomograms before the freezing, at the minimum temperature, and after the thawing, respectively, during the rapid cooling and rapid warming. In contrast to only extracellular freezing occurring during slow cooling, both extracellular freezing and intracellular freezing occurred during the rapid cooling. Intracellular ice formation occurred because the dehydration from the muscle fibers due to the growth of extracellular ice crystals was not sufficient to compensate for the rapid cooling rate, and consequently, the supercooling in the solution inside the cells caused ice nucleation.

Although the muscle fibers adhered to each other and were well-ordered before the freezing (Fig. 9a), during the cooling, extracellular ice crystals formed (Fig. 9b), similar to the behavior seen during slow cooling. However, these extracellular ice crystals were more slender (smaller in diameter) than those formed during the slow cooling. Furthermore, numerous fine ice crystals formed along the direction of the muscle fibers and along the myofibrils within the muscle fibers themselves (Fig. 9b). The muscle fibers were dehydrated, shrunk, and deformed. Extracellular ice crystals (solid white circles in Fig. 9b′ and b′-1) did not reach the upper

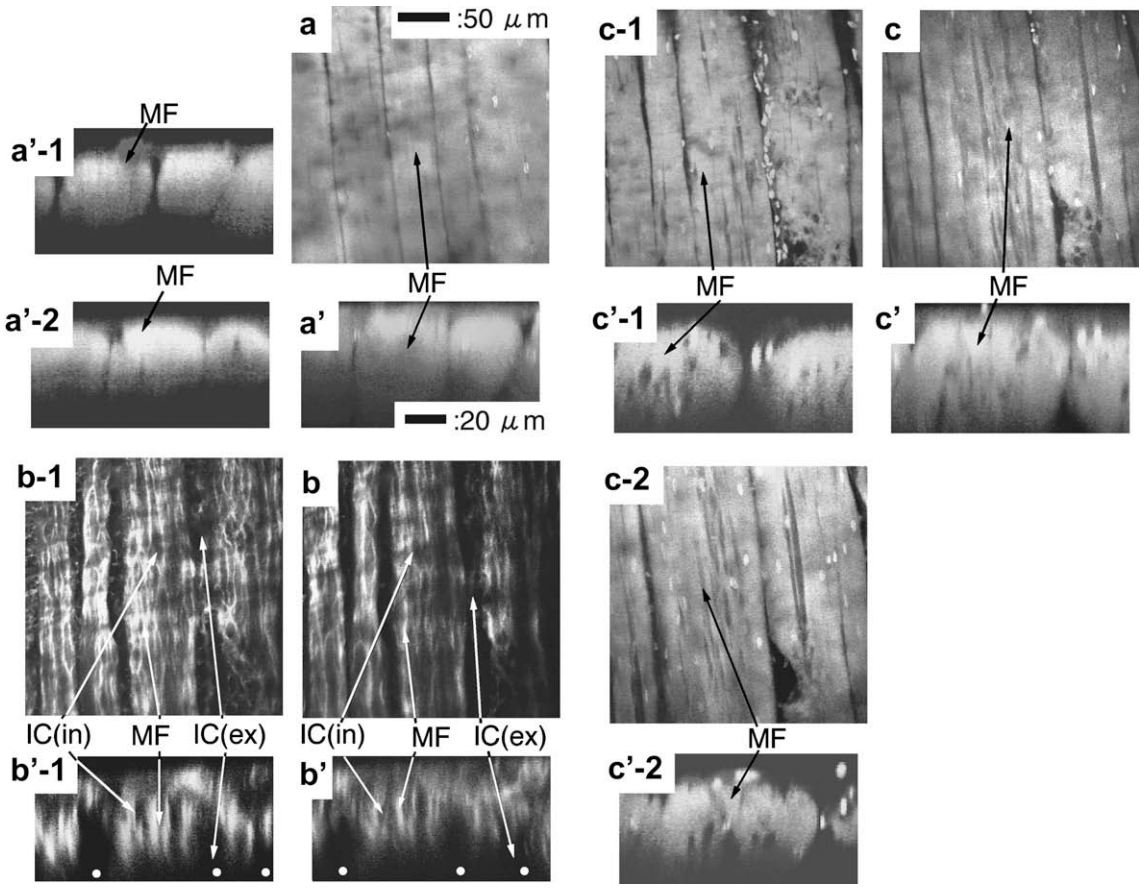

Fig. 9. Ice crystals and tissues during rapid cooling and rapid warming (H = 90 °C/min, W = 140 °C/min), (a) 10 °C (12.3 °C) (before freezing) (z = −20.3 μm), (b) −50 °C (−43.3 °C) (z = −23.7 μm), (c) 10 °C (12.0 °C) (after thawing) (z = −21.9 μm), (a′-1) y = 125.0 μm, (a′) y = 0 μm, (a′-2) y = −119.9 μm, (b-1) z = −11.9 μm, (b′-1) y = 12.8 μm, (b′) y = 0 μm, (c-1) z = −10.9 μm, (c-2) z = −30.7 μm, (c′-1) y = 125.0 μm, (c′) y = 0 μm, (c′-2) y = −94.4 μm.

surface of the sample. Compared to the other images (e.g., Fig. 9a′ and c′ and *x*–*z* section images in Fig. 5), both the *x*–*z* section images (Fig. 9b′ and b′-1) were indistinct probably due to light scattering by the numerous scattered fine ice crystals.

During the warming, extra- and intracellular ice crystals thawed and the muscle fibers reswelled and recovered in volume to some degree due to the inflow of water into the muscle fibers. After the thawing (Fig. 9c), cracks remained not only between the muscle fibers but also numerous small cracks remained in the muscle fibers themselves. The extra- and intracellular cracks were caused by the ice crystals. The images revealed that the tissues also incurred intracellular damage. Similar to the behavior of extracellular ice crystals, the cracks between the muscle fibers after thawing (Fig. 9c) were somewhat wider compared to those before freezing (Fig. 9a), but were narrower than those after slow cooling and rapid warming (Fig. 8).

Deformation of the muscle fibers after the rapid cooling and rapid warming (Fig. 9c) was less than that after the slow cooling and rapid warming (Fig. 8). After the slow cooling, each ice crystal was large and the ice crystals and cytoplasm of muscle fibers were unevenly distributed, thus resulting in large deformation of the muscle fibers due to dehydration and shrinkage. In contrast, after the rapid cooling, each ice crystal was small and particularly the intracellular ice crystals were fine and relatively evenly dispersed, thus resulting in less deformation of the muscle fiber itself.

4.2.3. Histological change in tissues due to freezing and thawing

Histological changes and damage in the tissues due to the freezing and thawing were also investigated by using staining to clarify the correlation to the above results from real-time 3D imaging by using the CLSM/dye method.

After the freezing and thawing, the tissues were morphologically investigated by masson-trichrome staining and hematoxylin-eosin staining. Fig. 10 shows representative results of the tissues stained by masson-trichrome as black-and-white photographs. Fig. 10a–c are horizontal section images parallel to the direction of muscle fibers, and Fig. 10a′, a″, b′, b″, c′ and c″ are perpendicular section images to the fibers. Fig. 10a′–c′ are images taken near the original smooth surface of the sample, whereas Figs. 10a″–c″ are those taken inside the sample.

Before the freezing (control) (Fig. 10a, a′, and a″), the muscle fibers with connective tissues were closely compacted and well-ordered, similar to the results from the CLSM observation. This state was similar between the part near the top and the inside of the sample. The numerous extremely fine cracks in the muscle fibers are artifacts.

Two different thermal protocols show characteristic histological changes as follows. After the slow cooling and rapid warming (Fig. 10b, b′, and b″), the effects of extracellular freezing were evident; muscle fibers had shrunk and were deformed, with large cracks between them. In the cracks, connective tissues had separated from the muscle fibers. In the section image (Fig. 10b and b′), the effect of intracellular ice crystals was also observed; a few large cracks remained locally in the muscle fibers.

In contrast, after the rapid cooling and rapid warming (Fig. 10c, c′, and c″), the effects of intracellular ice crystals were evident; namely, numerous small, fine cracks appeared in the muscle fibers. Although the rapid cooling and rapid warming protocol also showed effects of extracellular freezing, i.e., cracks between the muscle fibers, such cracks were narrower than those after the slow freezing and rapid warming. This is consistent with the smaller size of extracellular ice crystals formed during the rapid cooling and rapid warming, compared with those formed during the slow freezing and rapid warming. Also, the deformation of muscle fibers was less than that after the slow cooling and rapid warming protocol, and was rather similar to that of the control.

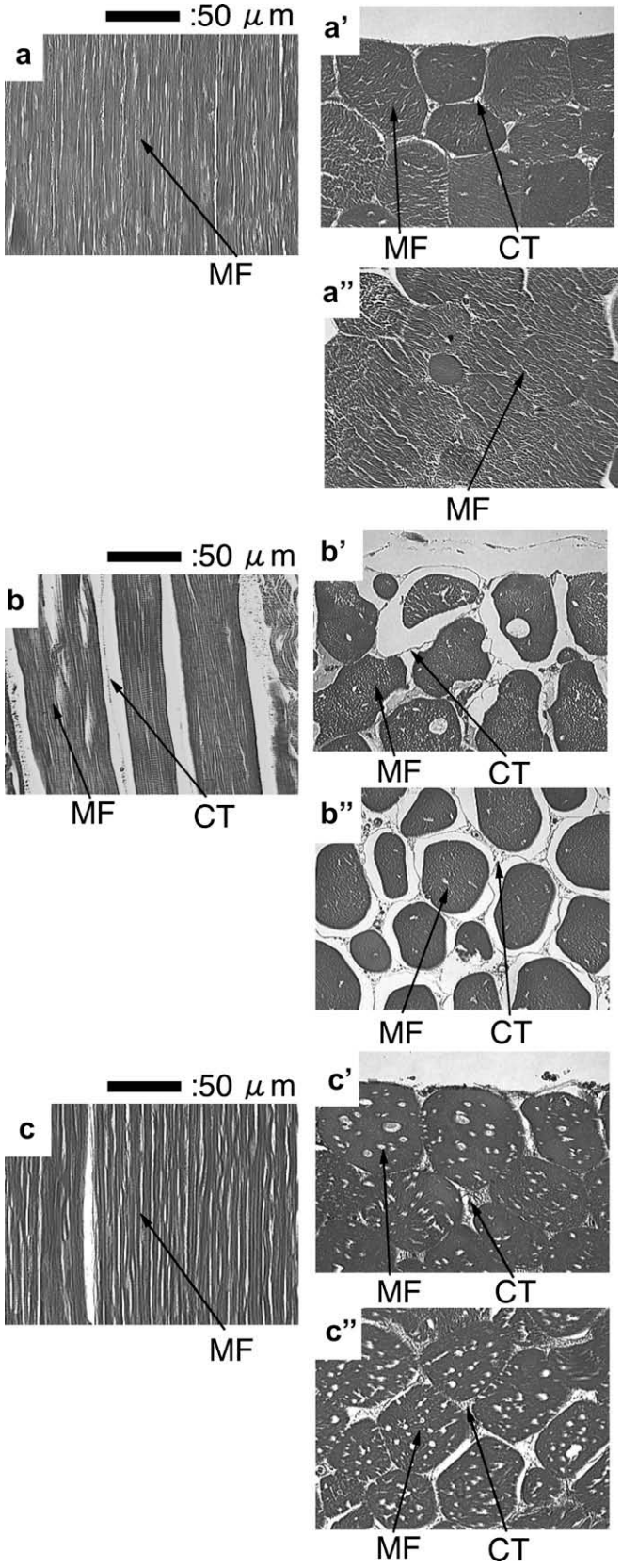

Fig. 10. Tissues stained by masson-trichrome after freezing and thawing, (a) control, (b) slow cooling and rapid warming (H = 1.0 °C/min, W = 140 °C/min), (c) rapid cooling and rapid warming (H = 95 °C/min, W = 130 °C/min).

Fig. 10 shows that the changes in tissue microstructure were basically similar between the top and inside of the sample for

the same thermal protocol and that the changes have distinctly different characteristics between the two thermal protocols. Therefore, the microstructure observed by the CLSM/dye method in the limited region near the top of the sample is representative of that inside the sample.

4.3. Post-thaw damage of tissues and evaluation of damage

The parameters used to evaluate the degree of post-thaw damage of biological tissues depend on the kinds of tissues and the purpose for preservation.

In the cryopreservation of foods and food materials, physical integrity (morphological integrity) is important for the preservation of texture. To maintain this integrity, the cooling rate should be increased to decrease the size of ice crystals and to disperse these ice crystals in the tissues. The rapid cooling decreases the amount of water removed from the cells during freezing, and consequently decreases the amount of post-thaw drip (i.e., water solution draining from thawed foods).

Rapid cooling causes both intra- and extracellular damages, however. Because intracellular freezing causes fatal damage, this type of freezing must be prevented when cryopreservation is used to preserve living cells and tissues, for example. Under extracellular freezing conditions, if the growth of ice crystals and the dehydration and shrinkage of the cells are excessive, fatal damage occurs. However, separation of adjoining muscle fibers also occurs in intercellular edema, even in tissues in a living body. Therefore, if the separation of muscle fibers caused by extracellular freezing is not excessive, the damage is not fatal.

5. Conclusion

The CLSM/dye method was applied to observe in detail the 3D microstructure of biological tissues (muscle tissues) during freezing and thawing. The results yielded the following conclusions:

(1) 3D behavior of ice crystals and cells during the freezing and thawing of muscle tissues can be investigated in real time by using CLSM with a fluorescent dye.
(2) During slow cooling and rapid warming, extracellular freezing is the typical freezing pattern for the tissues. In contrast, during rapid cooling and rapid warming, both intracellular freezing and extracellular freezing are the typical freezing patterns, and numerous ice crystals form in the muscle fibers. The ice crystals between the muscle fibers are more slender and smaller in the latter protocol than in the former protocol.
(3) Extracellular ice crystals, with slender shape along the direction of the fibers, tear the connective tissue between the muscle fibers, whereas intracellular ice crystals, with slender shape and finer size, tear the muscle fiber itself.
(4) Muscle fibers become dehydrated, shrink, and become deformed by the growth of any extra- and intracellular ice crystals. During the warming, ice crystals in the tissues liquefy, and the muscle fibers grow in volume due to the inflow of water into the fibers, but do not recover their original volume. After the thawing, irreversible cracks caused by ice crystals remain between the muscle fibers and in the muscle fibers themselves.
(5) Histologically morphological changes in the tissues due to freezing and thawing can be explained based on real-time 3D observation obtained by using the CLSM/dye method. Wide cracks between the muscle fibers are caused by extracellular freezing, and the width of these cracks corresponds to that of the ice crystals. Numerous fine cracks in the muscle fibers are caused by intracellular freezing.

Acknowledgements

The authors thank Dr. Hiroshi Kajigaya, Department of Veterinary Science, Nippon Veterinary and Life Science University, for his assistance and discussions. This work was supported by a Grant-in-Aid for Scientific Research (#09650222) from the Ministry of Education, Science, Sports and Culture of Japan, and Venture Business Laboratory, University of Tsukuba.

References

[1] H. Asou, S. Sumida, Low Temperature Medicine, Asukura Publishing, Tokyo, 1983 (in Japanese).
[2] H. Ishiguro, Application of low temperature in medicine and cryobiology, J. Jpn. Soc. Mech. Eng. 99 (927) (1996) 21–24 (in Japanese).
[3] A.A. Gage, J. Baust, Mechanisms of tissue injury in cryosurgery, Cryobiology 37 (1998) 171–186.
[4] J.J. McGrath, Low temperature injury processes, in: Advances in Bioheat and Mass Transfer, ASME HTD-vol. 268, 1993, pp. 125–132.
[5] R. Takai, Food processing in low temperature, J. Jpn. Soc. Mech. Eng. 99 (927) (1996) 17–20 (in Japanese).
[6] J. Bischof, C.J. Hunt, B. Rubinsky, A. Burgess, D.E. Pegg, Effect of cooling rate and glycerol concentration on the structure of the frozen kidney: assessment by cryo-scanning electron microscopy, Cryobiology 27 (1990) 301–310.
[7] B. Rubinsky, G. Onik, Cryosurgery: advances in the application of low temperature to medicine, Int. J. Refrig. 14 (1991) 190–199.
[8] Y.C. Song, C.J. Hunt, D.E. Pegg, Cryopreservation of the common carotid artery of the rabbit, Cryobiology 31 (1994) 317–329.
[9] M.W. Chaw, B. Rubinsky, Cryomicroscopic observation on directional solidification in onion cells, Cryobiology 22 (1985) 392–399.
[10] H. Ishiguro, K. Koike, Three-dimensional behavior of ice crystals and biological cells during freezing of cell suspensions, biotransport: heat and mass transfer in living systems, Ann. NY Acad. Sci. 858 (1998) 235–244.
[11] H. Ishiguro, K. Koike, Three-dimensional visualization of microstructure during extracellular-freezing of biological materials using confocal laser scanning microscope, in: Proc. of the 2nd Pacific Symposium on Flow Visualization and Image Processing, Pacific Center of Thermal-Fluids Engineering, Hawaii, PF121, 1999, pp. 1–10.